ANL-11/07

Hydrogen Production by Water Dissociation Using Ceramic Membranes

Annual Report for FY 2010

Energy Systems Division

About Argonne National Laboratory

Argonne is a U.S. Department of Energy laboratory managed by UChicago Argonne, LLC under contract DE-AC02-06CH11357. The Laboratory's main facility is outside Chicago, at 9700 South Cass Avenue, Argonne, Illinois 60439. For information about Argonne and its pioneering science and technology programs, see www.anl.gov.

Availability of This Report

This report is available, at no cost, at http://www.osti.gov/bridge. It is also available on paper to the U.S. Department of Energy and its contractors, for a processing fee, from:

U.S. Department of Energy
Office of Scientific and Technical Information
P.O. Box 62
Oak Ridge, TN 37831-0062
phone (865) 576-8401
fax (865) 576-5728
reports@adonis.osti.gov

ANL-11/07

Hydrogen Production by Water Dissociation Using Ceramic Membranes

Annual Report for FY 2010

by
U. (Balu) Balachandran, S.E. Dorris, J.E. Emerson,
T.H. Lee, Y. Lu, C.Y. Park, and J.J. Picciolo
Energy Systems Division, Argonne National Laboratory

February 7, 2011

Contents

I. OBJECTIVE 1

II. HIGHLIGHTS 1

III. INTRODUCTION 2

IV. RESULTS 3

Milestone 1: Fabricate and test thin-film OTM tubes using simulated coal gas streams to drive H_2 production by water splitting. 3

Milestone 2: Test use of simulated coal gas streams to drive H_2 production at low temperatures.. 7

Milestone 3: Continue to develop new membrane materials. 11

V. FUTURE WORK 19

PUBLICATIONS AND PRESENTATIONS 21

REFERENCES 22

Figures

1. Hydrogen production rates of LSCF thin-film tube and disk on porous LSCF substrate vs. CO concentration on oxygen-permeate side with humidified N_2 on hydrogen-generation side 5

2. Sequence of H_2 production rate measurements with LSCF thin-film tube 5

3. Hydrogen production rates of LSCF thin-film tube and disk vs. reciprocal temperature with various CO concentrations on oxygen-permeate side and moist N_2 on hydrogen-generation side 6

4. Area-specific H_2 production rates of LSCF thin-film tube and disk vs. reciprocal temperature using humidified N_2 on hydrogen-generation side. 7

5. Hydrogen production rate of 30-μm-thick, thin-film LSCF tube and 1-mm-thick, self-supporting BFZ1 tube vs. CO concentration on oxygen-permeate side of tube. 9

6. Hydrogen production rate of 30-μm-thick, thin-film LSCF tube and 1-mm-thick, self-supporting BFZ1 tube versus inverse temperature 9

7. Area-specific hydrogen flux and total hydrogen production rate of 1-mm-thick, self-supporting BFZ1 tube vs. flow rate of N_2 on hydrogen-generation side of tube. 10

8. Oxygen flux of BFO and BFZ0 membranes versus inverse temperature, measured with flowing He as sweep gas and air as feed gas 12

9. Time dependence of oxygen flux for 1.08-mm-thick $BaFeO_3$ membrane during phase transition at 847°C. 13

10. Oxygen flux of BFZ0, SFT1, and LSCF membranes versus inverse temperature 14

11. Oxygen flux of BFO, BFZ0, BFZ1, and BFZ2 disks versus inverse temperature 14

12. Hydrogen production rate of BFZ0, BFZ1, and BFZ2 disks versus inverse temperature, measured with 80% H_2/balance He on oxygen-permeate side and N_2 on hydrogen-generation side 15

13. Oxygen flux of BFO, BSFO, and SFO disks versus inverse temperature 16

14. Oxygen flux of various disk-type OTMs versus inverse temperature 17

15. Fracture-surface and plan view of BFZ1 thin films on BFZ1 porous substrates. 18

16. Fracture-surface and plan view of BSCF/Ag thin film on BSCF/Ag substrate 19

HYDROGEN PRODUCTION BY WATER DISSOCIATION USING CERAMIC MEMBRANES

ANNUAL REPORT FOR FY 2010

ARGONNE NATIONAL LABORATORY

Project Title: Hydrogen Production by Water Dissociation using Ceramic Membranes

NETL Project Manager: Richard Dunst

ANL Project PI: U. (Balu) Balachandran

B&R Code/Contract Number: AA-10-40-00-00-0/FWP 49347

Report Date: February 7, 2011

I. OBJECTIVE

The objective of this project is to develop dense ceramic membranes that can produce hydrogen via coal/coal gas-assisted water dissociation without using an external power supply or circuitry.

II. HIGHLIGHTS

1. Several OTM compositions [$La_{0.7}Sr_{0.3}Cu_{0.2}Fe_{0.8}O_{3-\delta}$ (LSCF), $BaFe_{0.90}Zr_{0.10}O_3$ (BFZ1), and $Ba_{0.5}Sr_{0.5}Cu_{0.2}Fe_{0.8}O_{3-\delta}$ (BSCF)] appear promising for producing hydrogen by water splitting at low temperatures (<700°C).

2. We met the milestone of fabricating and testing a thin-film tube using simulated coal gas to drive hydrogen production by water splitting. The milestone was met by testing an LSCF thin-film tube at 500-900°C.

3. We met the milestone of using simulated coal gas to drive hydrogen production by water splitting at low temperatures with a thin-film tube composed of LSCF and a dense, self-supporting tube composed of BFZ1.

4. Tests showed that BSCF gives a high oxygen flux at low temperature, but BSCF disks develop fine cracks after sintering. Cracks can be prevented by mixing BSCF with Ag, and BSCF/Ag composites give high oxygen flux at low temperature.

III. INTRODUCTION

This project grew from an effort to develop a dense ceramic membrane for separating hydrogen from gas mixtures such as those generated during coal gasification, methane partial oxidation, and water-gas shift reactions [1]. That effort led to the development of various cermet (i.e., ceramic/metal composite) membranes that enable hydrogen production by two methods. In one method, a hydrogen transport membrane (HTM) selectively removes hydrogen from a gas mixture by transporting it through either a mixed protonic/electronic conductor or a hydrogen transport metal. In the other method, an oxygen transport membrane (OTM) generates hydrogen mixed with steam by removing oxygen that is generated through water splitting [1, 2].

This project focuses on the development of OTMs that efficiently produce hydrogen via the dissociation of water. Supercritical boilers offer very high-pressure steam that can be decomposed to provide pure hydrogen using OTMs. Oxygen resulting from the dissociation of steam can be used for coal gasification, enriched combustion, or synthesis gas production. Hydrogen and sequestration-ready CO_2 can be produced from coal and steam by using the membrane being developed in this project. Although hydrogen can also be generated by high-temperature steam electrolysis, producing hydrogen by water splitting with a mixed-conducting membrane requires no electric power or electrical circuitry.

Water dissociates into oxygen and hydrogen at high temperatures by the reaction:

$$H_2O(g) \Leftrightarrow H_2 + \frac{1}{2}O_2$$

However, very low concentrations of hydrogen and oxygen are generated even at relatively high temperatures (e.g., 0.1 and 0.042% for hydrogen and oxygen, respectively, at 1600°C), because the reaction's equilibrium constant is small [3]. This shortcoming can be overcome at moderate temperatures by using a mixed-conducting (electron- and ion-conducting) membrane to remove either oxygen or hydrogen, which shifts the equilibrium toward dissociation. If an OTM is used to produce hydrogen, the hydrogen production rate depends directly on the rate at which oxygen is removed from the water dissociation zone, which depends on the OTM's oxygen permeability (a function of the OTM's electron and oxygen-ion conductivities), the surface oxygen exchange kinetics, and the oxygen partial pressure (pO_2) gradient across the OTM [4-7]. To obtain a high hydrogen production rate, mixed-conducting OTMs should exhibit high electron and oxygen-ion conductivities, possess good surface exchange properties, and be exposed to a high pO_2 gradient.

Others have used mixed-conducting OTMs to produce hydrogen by water dissociation, but the membranes had low electronic conductivity, and the hydrogen production rate was modest even at high temperature (e.g., 0.6 cm^3 (STP)/min-cm^2 at 1683°C [8]). We achieved a significantly higher hydrogen production rate using an OTM composed of an oxygen-ion conductor of cerium gadolinium oxide (CGO) and an

electronic conductor (Ni) [2]. The hydrogen production rate increased with increases in temperature, water partial pressure on the hydrogen-production side of the membrane, and oxygen chemical potential gradient across the membrane [2]. It also increased with decreasing membrane thickness, but it became limited by surface reaction kinetics for OTMs with thickness below ≈0.5 mm.

To be practical for hydrogen production, OTMs must give high hydrogen production rates and be available in a shape with a large active area, e.g., tubes. They must also remain chemically and mechanically stable in corrosive environments at elevated temperatures. All experimental milestones for FY 2010 were met by using OTMs that were developed at Argonne. This report summarizes progress during FY 2010 toward the fabrication of practical OTMs. The following milestones were established in the Field Work Proposal for FY 2010 as benchmarks in Argonne's efforts to develop practical OTMs:

1. Fabricate and test thin-film OTM tubes using simulated coal gas streams to drive H_2 production by water splitting.
2. Test use of simulated coal gas streams to drive H_2 production at low temperatures.
3. Continue to develop new membrane materials.

IV. RESULTS

Results are presented below in relation to the pertinent milestone for FY 2010.

Milestone 1. Fabricate and test thin-film OTM tubes using simulated coal gas streams to drive H_2 production by water splitting.

A 25-μm-thick $SrFeCo_{0.5}O_x$ (SFC2) film on a porous SFC2 substrate gave the highest hydrogen production rate to date for an Argonne OTM, 17.4 cm^3/min-cm^2 at 900°C [9], but a phase transition dramatically reduced this material's hydrogen production rate below 825°C. To achieve high hydrogen production rates at low temperatures (<700°C), we are developing alternative OTM compositions that do not undergo such phase transitions, and we are developing techniques for reducing the thickness of OTMs by making thin films on porous substrates. Alternative OTMs with potential for producing hydrogen at low temperatures include $La_{0.7}Sr_{0.3}Cu_{0.2}Fe_{0.8}O_{3-\delta}$ (LSCF) and compositions in the Ba-Fe-Zr-O (BFZ) system. Following are results from hydrogen production rate measurements that were made with a thin-film LSCF tube on a porous LSCF substrate.

We prepared LSCF powder by conventional solid-state synthesis using La_2O_3 from Alfa Aesar (99.999%), $SrCO_3$ from Aldrich (99.9+%), CuO from Johnson Matthey (99.999%), and Fe_2O_3 from Alfa Aesar (99.99%) as the starting materials. Stoichiometric amounts of the starting materials were mixed and milled with zirconia balls in isopropyl alcohol (IPA) for two days. The mixture was dried, calcined at 900°C for 5 h in air, and then ball milled. To prepare porous supports for tubular thin films, LSCF powder was

mixed with carbon (20 wt. %) in IPA, ball milled overnight, and dried. Tubes were made by pressing the powder mixture at 10,000-15,000 psig inside a rubber mold (Trexler Rubber) with a stainless steel mandrel in a cold isostatic press (Engineered Pressure System) and firing at 1050°C for 10 h in ambient air.

Thin films were coated on the tube surface by painting with an LSCF slurry. The slurry was prepared by mixing LSCF powder with a binder (polyvinyl butyral), plasticizer, and solvent (α-terpineol). After painting the slurry onto a tube, the sample was dried at 80°C for 1 h and heated at 1100-1140°C for 10 h in air. After firing, the tube had an outside diameter of ≈1 cm, inside diameter of ≈0.7 cm, and length of ≈5.1 cm.

Before the hydrogen production rate was measured, each tube was tested for pinholes and/or microcracks by checking for penetration of the thin film by IPA. After the hydrogen production measurements, scanning electron microscopy (SEM) showed that the LSCF thin film had a thickness of ≈30 μm.

The hydrogen production rate of the LSCF tube was measured at 500-900°C. During the measurements, ultrahigh purity (UHP) N_2 was flowed through water and then over the outside of the tube, called the hydrogen-generation side. Then, CO-containing gases (99.5% CO or CO/CO_2 mixtures) were flowed on the inside of the tube, called the oxygen-permeate side. Both gases flowed at a rate of 150 cm^3/min. The steam partial pressure (pH_2O) was fixed at 0.49 atm on the hydrogen-generation side by controlling the water temperature at 81°C. An Agilent gas chromatograph was used to measure the hydrogen concentration on the hydrogen-generation side of the membrane.

Figure 1 compares the hydrogen production rates of the LSCF thin-film tube and an LSCF thin-film disk. The data for the disk were reported previously [10]. The hydrogen production rate is plotted over the range 500-900°C versus the CO concentration on the oxygen-permeate side of the membranes. The active area was ≈1.3 cm^2 for the disk and ≈15.3 cm^2 for the tube. The hydrogen production rate of the tube was three times higher than that of the disk at 900°C and 15 times higher at 600°C. Considering that the disk's hydrogen production rate was ≈5.5 cm^3/min, and the tube's active area was >12 times higher than that of the disk, the hydrogen production rate of the tube at 900°C (≈19.5 cm^3/min using 99.5% CO) was not as high as expected.

Two factors might contribute to the tube's hydrogen production rate being lower than expected at 900°C. The tubular thin film was slightly thicker than the disk-type film (≈30 vs. ≈20 μm), and concentration polarization was evident. The hydrogen production rate of the tube increased ≈25% (to 24.6 cm^3/min) when the flow rate of humidified N_2 was increased to 300 cm^3/min on the hydrogen-generation side while the flow rate of CO on the oxygen-permeate side was left at 150 cm^3/min. When the flow rate of CO on the oxygen-permeate side was increased to 300 cm^3/min while the flow rate of humidified N_2 on the other side was kept at 150 cm^3/min, the hydrogen production rate did not change significantly. The fact that doubling the flow rate of N_2 significantly increased the hydrogen production rate, but doubling the flow rate of CO did not, indicates that concentration polarization is more severe on the hydrogen-generation side.

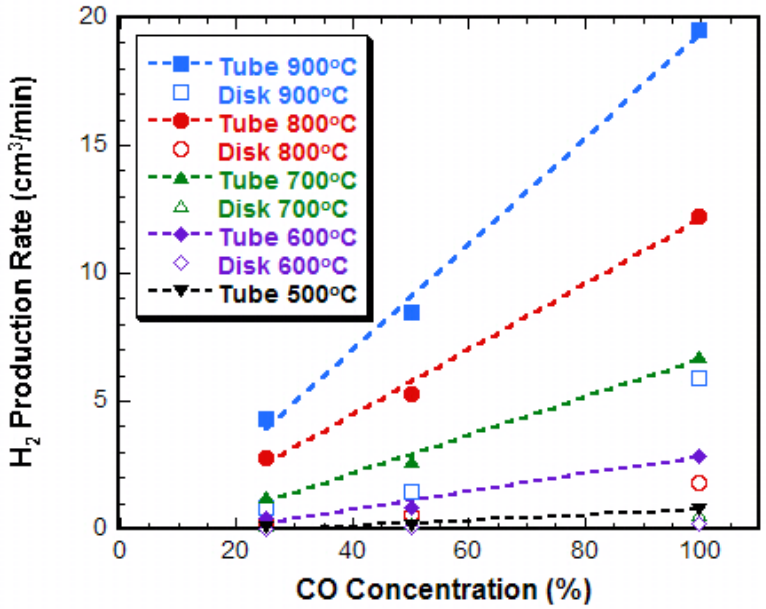

Fig. 1 Hydrogen production rates of LSCF thin-film tube and disk on porous LSCF substrate vs. CO concentration on oxygen-permeate side with humidified N_2 (pH_2O = 0.49 atm) on hydrogen-generation side.

After the hydrogen production rate was measured in tests using 99.5% CO and CO/CO_2 mixed gases from 900°C to 500°C, the hydrogen production rate was measured again under the initial conditions (at 900°C with 99.5% CO on the oxygen-permeate side and humidified N_2 on the hydrogen-generation side, both gases flowing at 150 ml/min). Figure 2 shows the sequence of measurements that were made with the tubular thin film. The re-measured value for the hydrogen production rate (19.6 cm^3/min) was essentially identical to the initial value (19.5 cm^3/min), indicating that the hydrogen production rate is reproducible, and that the LSCF thin film was stable during ≈80 h of testing.

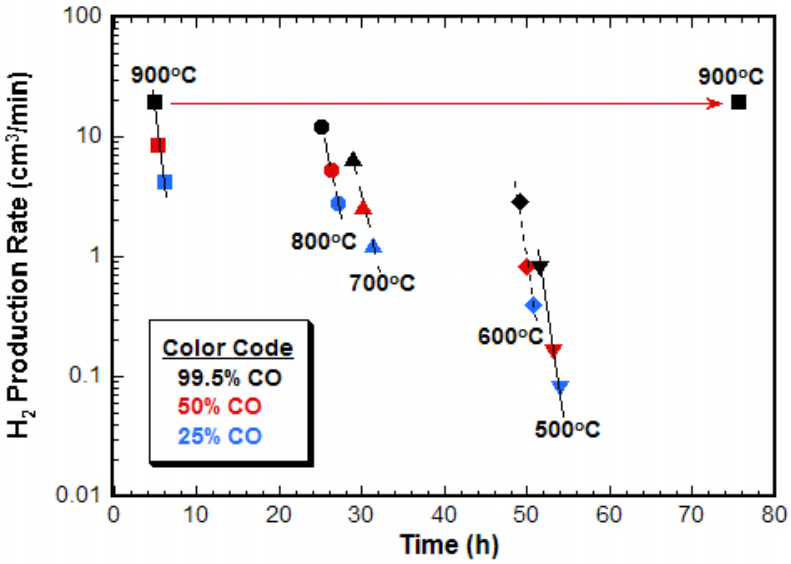

Fig. 2 Sequence of H_2 production rate measurements with LSCF thin-film tube.

Figure 3 shows the hydrogen production rate of the tubular LSCF thin film versus reciprocal temperature for different CO concentrations on the oxygen-permeate side. The hydrogen production rate of an LSCF thin-film disk [10] is included as a reference. For both the tube and the disk, the hydrogen production rate decreased as the CO concentration decreased on the oxygen-permeate side, because the hydrogen production rate depends directly on the oxygen flux through the membrane, which is driven by the reaction between the CO/CO_2 mixture and oxygen emerging from the membrane. As the CO concentration decreases, the CO/CO_2 mixture becomes less reactive toward oxygen and the oxygen flux decreases. The data for both the tube and the disk suggest that significant quantities of hydrogen could be produced by using product streams from coal gasification to drive the dissociation of water. Through the reverse Boudouard reaction,

$$CO_2 + C = 2\ CO,$$

CO_2 could be used to generate gas streams that could be used to produce additional hydrogen via water splitting.

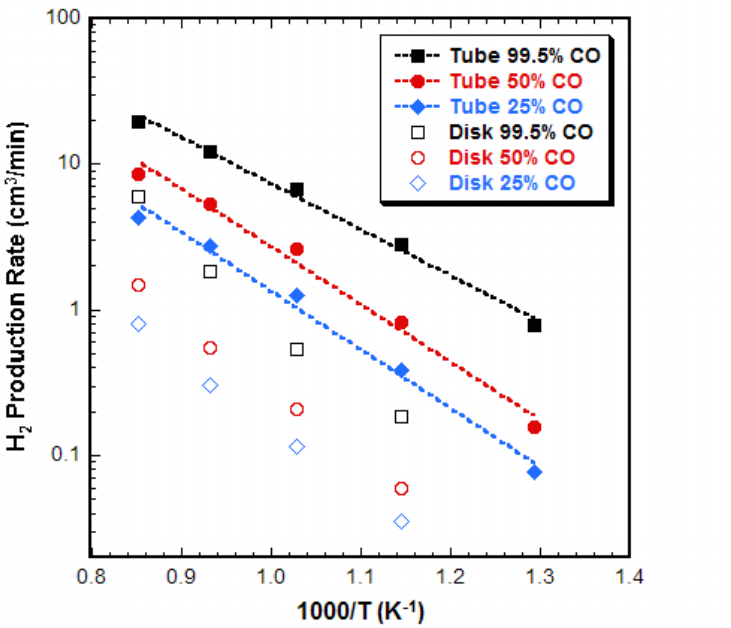

Fig. 3 Hydrogen production rates of LSCF thin-film tube and disk vs. reciprocal temperature with various CO concentrations on oxygen-permeate side and moist N_2 (pH_2O = 0.49 atm) on hydrogen-generation side.

Figure 4 plots the area-specific hydrogen production rate versus inverse temperature for the thin-film tube and disk in tests using three CO concentrations on the oxygen-permeate side of the film. The inset gives the type of sample (tube or disk), the CO concentration on the oxygen-permeate side of the film, and the apparent activation energy (E_a). Although the tube and disk had the same membrane composition, their activation energies differ with the same CO concentration due to concentration polarization effects.

Because concentration polarization is promoted by conditions that favor a high oxygen flux and the oxygen flux increases with CO concentration, the difference in E_a for the disk and film increases with the CO concentration. With 99.5% CO flowing on the oxygen-permeate side, the difference was 0.39 eV (1.02 eV for disk versus 0.63 eV for tube), but it decreased to 0.16 eV with 50% CO on the oxygen-permeate side and 0.11 eV with 25% CO. For a given gas, the area-specific hydrogen production rates of the disk and tube differed the most at high temperature, where the oxygen flux was highest, and the difference decreased as the temperature (and flux) decreased.

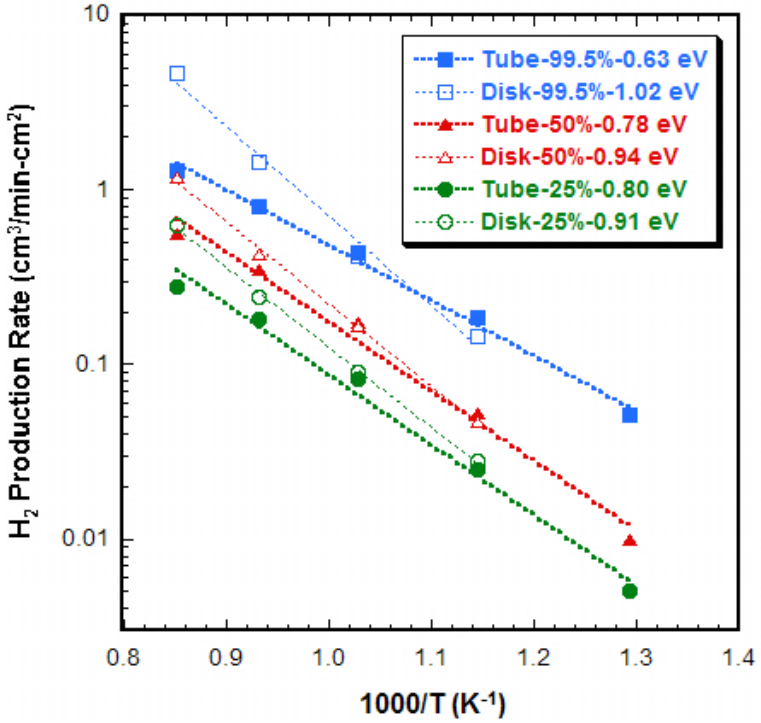

Fig. 4 Area-specific H_2 production rates of LSCF thin-film tube and disk vs. reciprocal temperature using humidified N_2 (pH_2O = 0.49 atm) on hydrogen-generation side. Inset gives sample type, CO concentration on oxygen-permeate side, and apparent activation energy.

Milestone 2. Test use of simulated coal gas streams to drive H_2 production at low temperatures.

To achieve high hydrogen production rates at low temperatures (<700°C), the OTM must provide a high oxygen flux. A high oxygen flux can be achieved by decreasing the thickness of the OTM or by using an OTM with superior intrinsic oxygen transport properties. Milestone 2 was met with a tubular LSCF thin film and with a self-supporting tube composed of $BaFe_{0.90}Zr_{0.10}O_3$ (BFZ1). Results are shown here from hydrogen production rate measurements with the BFZ1 tube at 600-900°C. The results for the LSCF thin-film tube are discussed above, but are also shown here for direct comparison with the results for the BFZ1 tube.

We prepared BFZ1 by partially substituting Zr for Fe in $BaFeO_3$ (BFO). Like SFC2, BFO exhibits high oxygen flux at high temperature but undergoes a phase transition that limits the flux below ≈860°C. With the Zr substitution, we hoped to achieve high oxygen flux and hydrogen production rates at low temperatures by retaining BFO's high-temperature cubic phase. The oxygen flux of BFZ1 is approximately one to two orders of magnitude higher than that of LSCF over the whole temperature range.

We prepared BFZ1 powder by conventional solid-state synthesis. Proper amounts of $BaCO_3$, Fe_2O_3, and ZrO_2 were ball-milled for one day with zirconia media in IPA. After drying, the mixture was heated at 850°C for 20 h in air and ball-milled for one day. The dried powder was heated again at 880°C for 20 h and then ball-milled. Dense tubes, closed on one-end, were fabricated by pressing BFZ1 powder in a cold isostatic press (Engineered Pressure Systems) at 10,000-15,000 psig in a rubber mold (Trexler Rubber) with a stainless steel mandrel. Tubes were sintered in flowing nitrogen for 6 h at 1330°C. The tube we tested had outside diameter of 0.96 cm, inside diameter of 0.75 cm, and length of 5.74 cm, with active area ≈17.3 cm^2 on the outside and ≈13.5 cm^2 on the inside.

Before the hydrogen production rate was measured, the tube was tested for flaws by filling it with IPA and checking for penetration by the IPA. Penetration by even a small amount of IPA is visible as darkening of the tube's surface and indicates the presence of cracks or interconnected porosity. If the IPA test revealed no flaws, the tube's hydrogen production rate was measured with a spring-loaded test fixture that squeezed a gold gasket between the OTM tube and an alumina tube to produce a gas-tight seal. During hydrogen production rate measurements, gas flowed through the alumina tube to the inside of the OTM tube.

To measure the hydrogen production rate, ultrahigh purity (UHP) N_2 flowed through water at 81°C to give pH_2O=0.49 atm on the hydrogen-generation side of the membrane. Various gases (e.g., CO/CO_2 or H_2/He mixtures) that are reactive with oxygen were flowed over the oxygen-permeate side of the OTM to drive the oxygen diffusion that promotes hydrogen production. The hydrogen production rate was measured with gas flow rates of 150-450 cm^3/min on the hydrogen-generation side and 150 cm^3/min on the oxygen-permeate side at 600-900°C. To measure the hydrogen production rate, the hydrogen concentration on the hydrogen-generation side was measured with an Agilent 6890 gas chromatograph (GC).

Figure 5 plots the H_2 production rate of a dense BFZ1 tube at 600-900°C vs. the CO concentration on the tube's oxygen-permeate side; CO_2 composed the balance of each gas. The hydrogen production rate of a tubular LSCF thin film at 500-900°C, shown in Fig. 4, is also plotted for comparison. Figure 6 plots the hydrogen production rate vs. inverse temperature for both tubes for each gas that was flowed on the oxygen-permeate side (25, 50, and 99.5% CO), and shows the activation energy that was calculated. Figure 7 plots the area-specific and total hydrogen production rate for the BFZ1 tube vs. flow rate of N_2 (pH_2O=0.49 atm) on the hydrogen-generation side with 72% CO/balance CO_2 flowing at a fixed flow rate (150 cm^3/min) on the oxygen-permeate side.

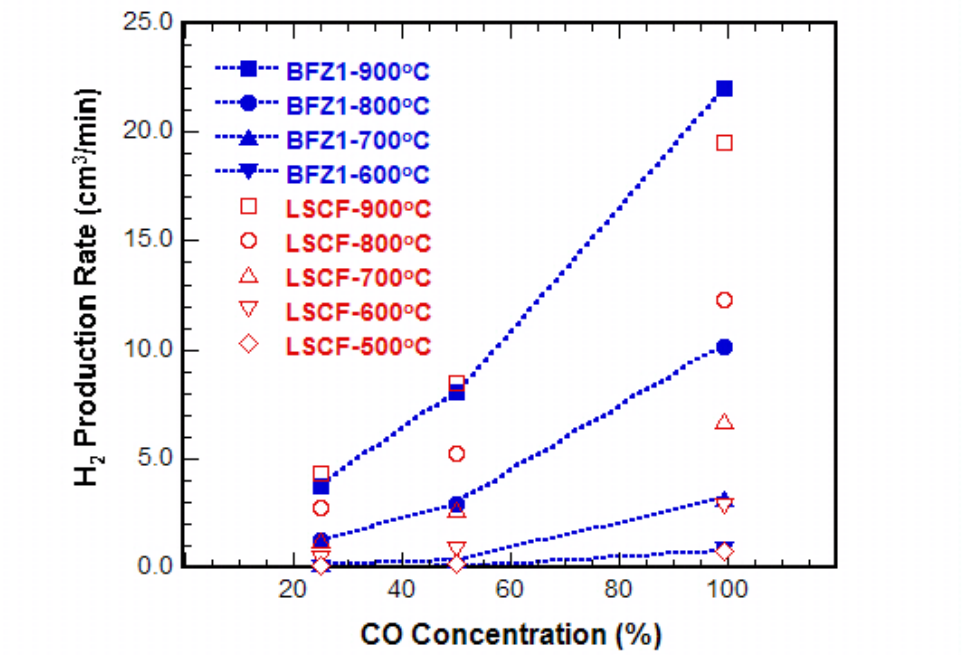

Fig. 5 Hydrogen production rate of 1-mm-thick, self-supporting BFZ1 tube and 30-μm-thick, thin-film LSCF tube vs. CO concentration (balance CO_2) on oxygen-permeate side of tube.

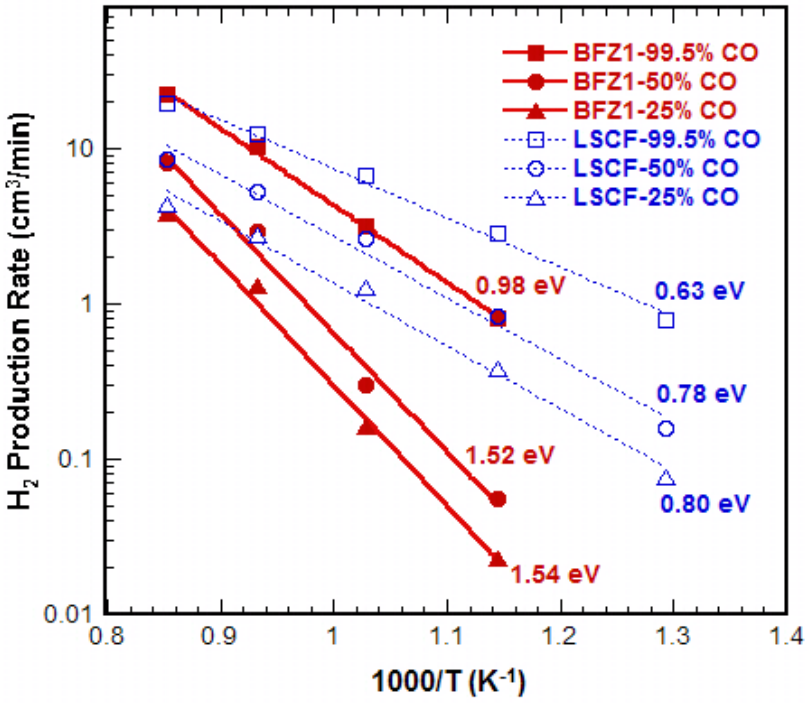

Fig. 6 Hydrogen production rate of 1-mm-thick, self-supporting BFZ1 tube and 30-μm-thick, thin-film LSCF tube versus inverse temperature. Activation energy (E_a) is shown for each plot. Inset gives CO concentration (balance CO_2) on oxygen-permeate side of tube during measurements.

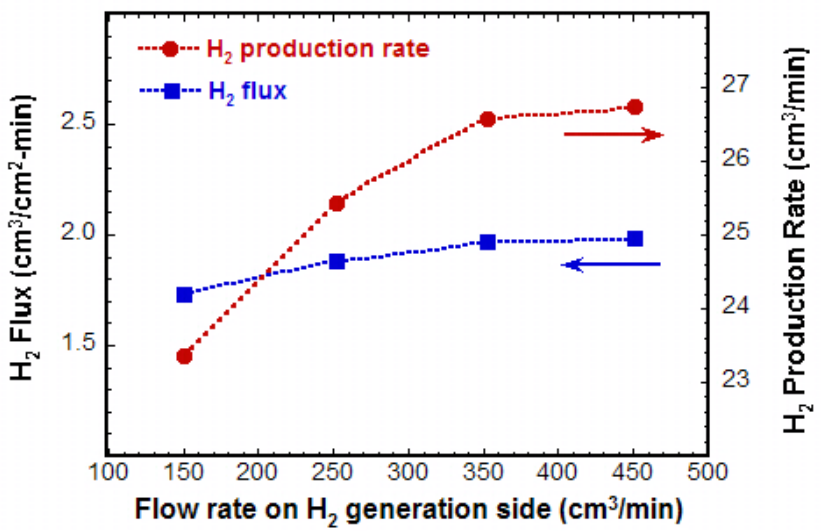

Fig. 7 Area-specific hydrogen flux ($cm^3/min\text{-}cm^2$) and total hydrogen production rate (cm^3/min) of 1-mm-thick, self-supporting BFZ1 tube vs. flow rate of N_2 (0.49 atm H_2O) on hydrogen-generation side of tube.

For both tubes, increasing the CO concentration on the oxygen-permeate side increased the hydrogen production rate (Fig. 5). This effect is expected because the hydrogen production rate depends directly on the OTM's oxygen flux, which is driven by reaction between the CO/CO_2 mixture and oxygen emerging from the membrane. As the CO concentration increased, the CO/CO_2 mixture became more reactive toward oxygen, and the oxygen flux increased, which increased the hydrogen production rate.

Due to BFZ1's superior oxygen transport properties, its hydrogen production rate at 900°C was comparable to that for the LSCF tube (Fig. 5), even though BFZ1 was much thicker (≈1000 μm vs. ≈30 μm). The LSCF thin-film tube gave the higher hydrogen production rate at lower temperatures (<900°C), however, as a result of BFZ1's higher activation energy for hydrogen production (Fig. 6). The change in activation energy with CO concentration can be related to the effects of concentration polarization. Because concentration polarization is promoted by conditions that favor a high oxygen flux (i.e., high temperature and/or high CO concentration), it reduces the hydrogen production rate the most at high temperature, which causes a decrease in the apparent activation energy. This effect is the most prominent with a high CO concentration on the oxygen-permeate side. As a result, the activation energy decreases as the CO concentration increases.

As the flow rate of humidified N_2 was increased on the hydrogen-generation side of the membrane, the hydrogen production rate increased significantly (Fig. 7) due to the effects of concentration polarization. Likewise, the hydrogen production rate of the LSCF thin-film tube increased ≈25% when the flow rate of humidified N_2 was increased while the flow rate of CO on the oxygen-permeate side was unchanged. When the flow rate of CO on the oxygen-permeate side was increased without changing the flow rate of humidified N_2, the hydrogen production rate changed very little, indicating that concentration polarization was more severe on the hydrogen-generation side.

Milestone 3. Continue to develop new membrane materials.

Conventional solid-state synthesis was used to prepare powders of $BaFeO_3$ (BFO), $BaFe_{0.975}Zr_{0.025}O_3$ (BFZ0), $BaFe_{0.9}Zr_{0.1}O_3$ (BFZ1), $BaFe_{0.8}Zr_{0.2}O_3$ (BFZ2), $SrFeO_3$ (SFO), $Ba_{0.5}Sr_{0.5}FeO_3$ (BSFO), and $Ba_{0.5}Sr_{0.5}Cu_{0.2}Fe_{0.8}O_{3-\delta}$ (BSCF). Proper amounts of $BaCO_3$, Fe_2O_3, $SrCO_3$, CuO, and ZrO_2 were ball-milled for one day with zirconia media in IPA. After the mixture was dried, it was heated at 800-880°C for 10-20 h in air and ball-milled for one day as before. Powders were pressed uniaxially into disks (7/8 in. dia.) and sintered for 6 h in 100 ppm H_2/balance N_2 or in ambient air at 1250°C (BFO, BFZ0) or 1350°C (BFZ1, BFZ2). The SFO disk was sintered for 10 h in 100 ppm H_2/balance N_2 at 1300°C; the BSFO disk was sintered in air at 1200°C for 6 h; and BSCF disks were sintered in ambient air for 10 h at 950-1000°C.

The BSCF disks developed fine cracks after sintering; however, cracks did not develop when BSCF was mixed with Ag powder (99.9%, 0.7-1.3 μm, Alfa-Aesar) in a mortar and pestle to prepare composites with 10-40 vol.% Ag. The BSCF/Ag powder mixtures were pressed uniaxially into disks (≈1 in. dia) and sintered for 10 h at ≈930°C in ambient air.

The oxygen flux was measured by sealing a polished disk to the end of an Al_2O_3 tube with a spring-loaded assembly that squeezed a gold ring between the sample and the Al_2O_3 tube. During the measurements, air and UHP He were flowed (150 cm^3/min) on the feed and sweep sides of the membrane, respectively. The oxygen and nitrogen concentrations in the sweep gas were measured with an Agilent gas chromatograph, and the nitrogen concentration was used to correct for leakage through the gas seal.

Ba-Fe-Zr-O: Figure 8 shows the oxygen flux as a function of inverse temperature for the BFO and BFZ0 membranes. Both plots show distinct changes in slope, but at significantly different temperatures, ≈850-870°C for BFO and ≈750-775°C for BFZ0. Watanabe et al. [11] and Zhu et al. [12] also noted a change in the slope of BFO's oxygen permeation rate versus inverse temperature. Based on high-temperature x-ray diffraction measurements, Watanabe ascribed the change in slope to a transition from a cubic phase at high temperature to a low-temperature triclinic phase. If the slope changes in Fig. 8 are also attributed to the cubic-to-triclinic phase transition, we find that the transition for BFO occurs at a considerably higher temperature (≈850-870°C) than the transition temperatures reported by Watanabe et al. (≈700°C) and Zhu et al. (≈810°C).

Considering that the samples were relatively thick (≈1 mm), BFO and BFZ0 both gave very high oxygen flux values (>1 cm^3/min-cm^2) at temperatures above the phase transition. Doping the Fe site of BFO with a small amount of Zr did not reduce the oxygen permeation rate above the phase transition temperature, but it lowered the phase transition temperature by ≈100°C. Our data for BFZ0 agree well with values reported by Watanabe et al. [11] at temperatures above the transition temperature, but our values are lower at temperatures below the transition temperature. Watanabe et al. did not observe any change in the slope for BFZ0, whereas our data show a phase transition that was shifted to a significantly lower temperature compared to BFO.

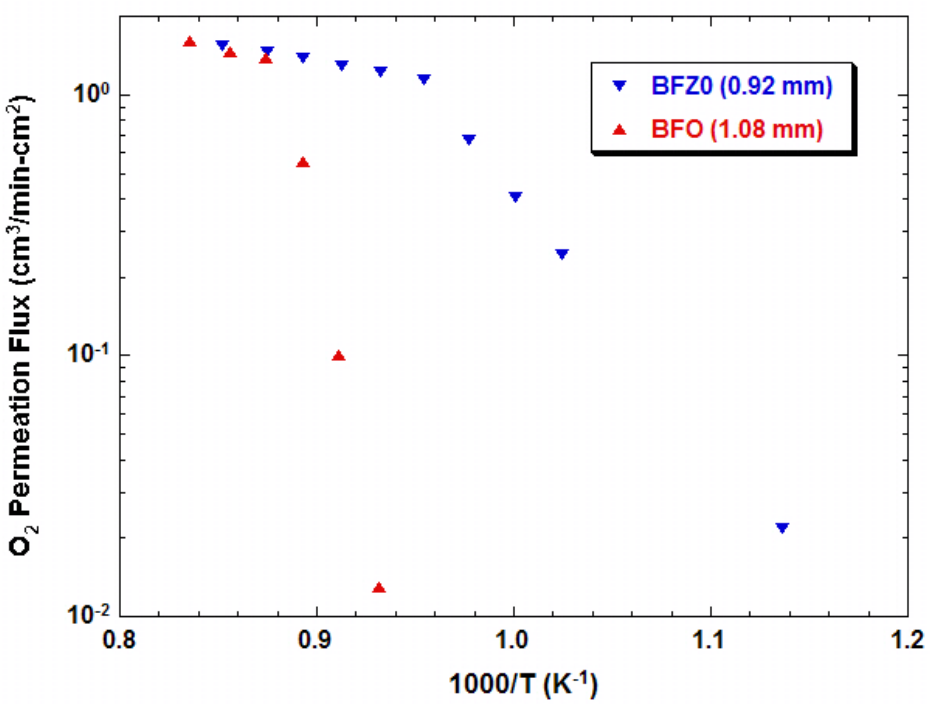

Fig. 8 *Oxygen flux of BFO and BFZ0 membranes versus inverse temperature, measured with flowing He (150 ml/min) as sweep gas and air (150 ml/min) as feed gas. Figure inset gives membrane thickness.*

To investigate the kinetics of the cubic-to-triclinic phase transition, the oxygen flux of BFO was measured versus time during the phase transition. Figure 9 shows the time dependence of the oxygen flux for a 1.08-mm-thick BFO membrane at 847°C. The measurements were made with flowing He (50 ml/min) as the sweep gas and began after the temperature was lowered from 870°C (above the transition temperature) to 847°C (below the transition temperature). The oxygen permeation rate changed very slowly after the change in temperature, requiring ≈50 h to approach a stable value and indicating that the cubic-to-triclinic phase transition occurs very slowly. In comparison, the oxygen permeation rate reached stable values relatively quickly (within ≈1 h) at temperatures above the transition temperature.

Because the oxygen flux reaches a steady-state value very slowly during the phase transition (Fig. 9), the apparent change in slope depends on the speed at which the flux measurements are made. Watanabe et al. [11] and Zhu et al. [12] measured the oxygen flux within 2-3 h of changing the membrane temperature, which is not sufficient time to reach steady-state values at temperatures below the transition temperature, according to Fig. 9. Oxygen flux measured before the attainment of steady state would be subject to a large uncertainty. Large uncertainty in the flux values measured below the transition temperature might explain why the transition temperature we report is significantly higher than those reported by Watanabe et al [11] and Zhu et al. [12], and why Watanabe et al. did not report a slope change for the oxygen permeation rate for BFZ0.

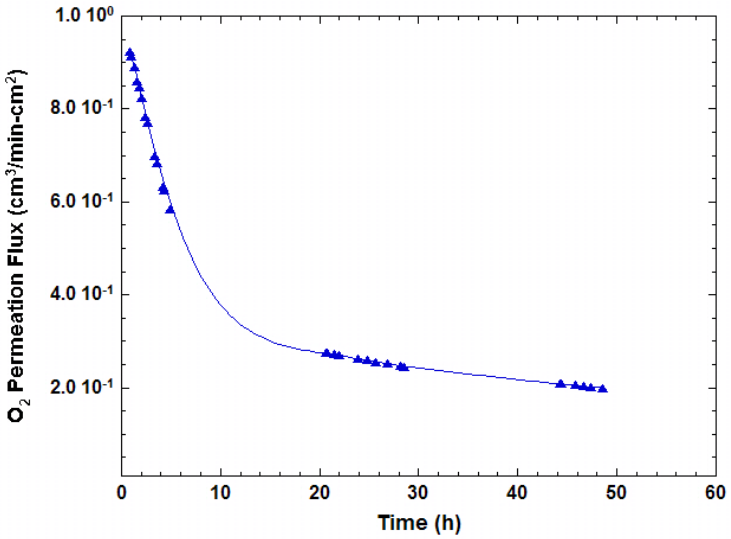

Fig. 9 Time dependence of oxygen flux for 1.08-mm-thick $BaFeO_3$ membrane during phase transition at 847°C. Sweep gas during measurement was He flowing at rate of 50 ml/min.

Figure 10 compares the temperature dependence of the oxygen flux for relatively thick (≈1 mm) BFZ0 with that of $Sr_{1.0}Fe_{0.9}Ti_{0.1}O_x$ (SFT1) and LSCF membranes. Measurements were made while flowing He as the sweep gas and air as the feed gas (150 ml/min). The flux of BFZ0 is an order of magnitude higher than that of LSCF over the whole temperature range, and is very high (>1 cm^3/min-cm^2) at temperature ≥775°C. Based on its high oxygen flux, BFZ0 appears promising for applications at low temperatures (<700°C); therefore, we will measure its hydrogen production rate via water dissociation. We will increase the Zr content in an effort to further decrease the transition temperature and obtain even higher oxygen flux at low temperatures.

Figure 11 shows the oxygen flux versus inverse temperature for BFO, BFZ0, BFZ1, and BFZ2 disks sintered in air, with the measured flux normalized for a 1-mm thickness; the figure inset gives the actual thickness of each sample. The oxygen flux for all four membranes decreases as temperature is decreased. The plots for BFO and BFZ0 each show a distinct change in slope, which is attributed to a transition between high-temperature cubic and low-temperature triclinic phases. The plots for BFZ1 and BFZ2 show less distinct slope changes, which occur at lower temperatures.

The slope changes for BFZ1 and BFZ2 might be caused by cubic-to-triclinic phase transitions; however, the changes for BFZ1 and BFZ2 are much more gradual, possibly indicating a different cause for the changes. X-ray diffraction (XRD) measurements [11] showed that disks sintered in air were single phase if they had ≤10 mol.% Zr, but an impurity phase was present in disks with >15 mol.% Zr. Detection of an impurity phase in materials with higher Zr content suggests that BFZ1 and BFZ2 might also contain an impurity phase that could affect the oxygen flux and cause the slope changes for BFZ1 and BFZ2. To understand the cause of the slope changes for Zr-doped $BaFeO_3$, XRD measurements at room temperature and high temperature would be helpful.

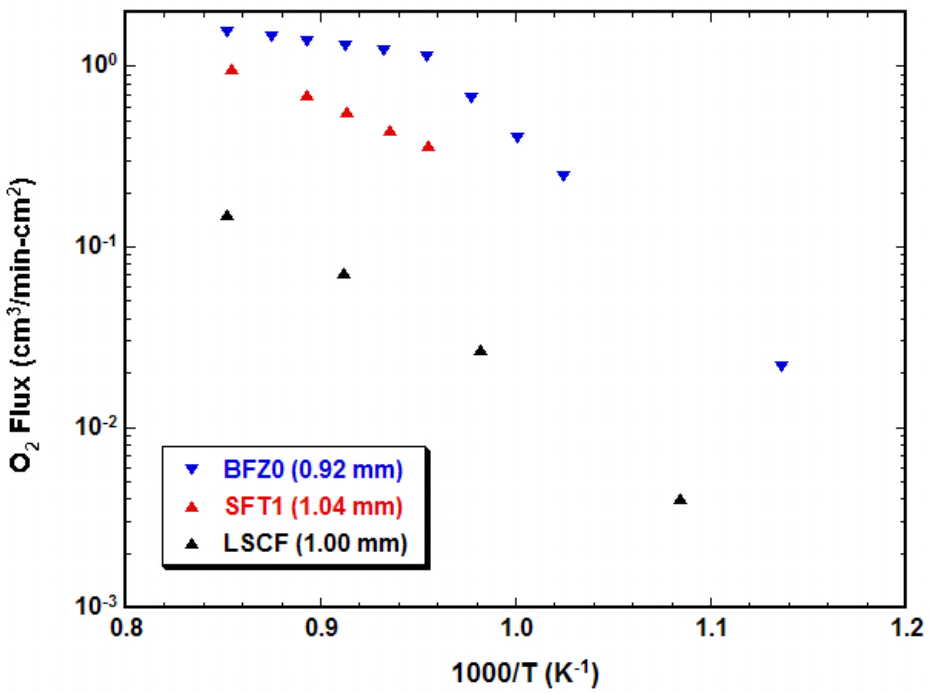

Fig. 10 Oxygen flux of BFZ0, SFT1, and LSCF membranes versus inverse temperature. Figure inset gives membrane thickness.

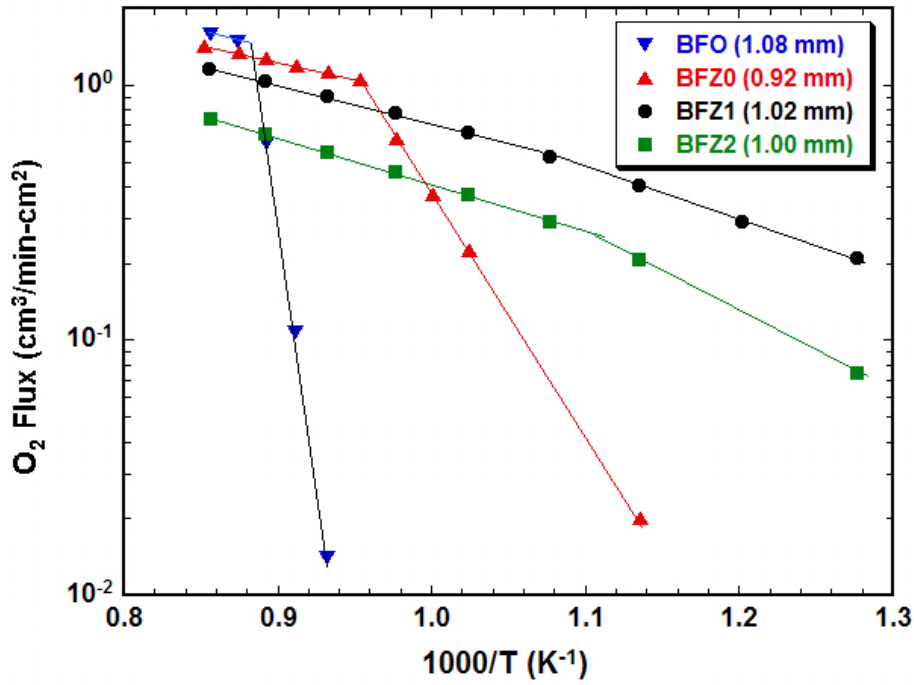

Fig. 11 Oxygen flux (normalized for thickness of 1.0 mm) of BFO, BFZ0, BFZ1, and BFZ2 disks versus inverse temperature. Inset gives measured membrane thickness.

Substituting Zr for Fe in BFO decreased the oxygen flux at temperatures above the inflection points (Fig. 11), but it increased the oxygen flux below the inflection points by lowering the apparent activation energy. Compared to BFO, BFZ1 gave ≈27% lower flux at 900°C, but unlike BFO, it retained a high flux up to 510°C (≈0.2 cm^3/min-cm^2). With higher Zr content, BFZ2 also gave a lower oxygen flux at 900°C, compared to BFO and BFZ0, but also retained a high flux up to 510°C. The oxygen flux of BFZ2 was ≈37% lower than that of BFZ1 at 900°C and ≈65% lower at 510°C. The decrease in oxygen flux might result from a decrease in oxygen conductivity caused by doping with zirconium. Substituting Zr for Fe should decrease the concentration of oxygen vacancies, thereby decreasing the oxygen conductivity, because the oxidation state of Fe is predominantly +3, whereas that of Zr is +4. Zirconium doping had little effect on the apparent activation energy for oxygen flux at temperatures above the inflection point, but it significantly decreased the activation energy below the inflection point. With lower activation energy, samples with higher Zr content gave much higher oxygen flux at low temperature.

Figure 12 shows the hydrogen production rate for BFZ0, BFZ1, and BFZ2 disks at 650-900°C, with all results normalized for a membrane thickness of 1.0 mm. The figure inset gives the actual thickness and apparent activation energy for each sample. All disks were sintered in 100 ppm H_2/balance N_2 to minimize large volume changes that can occur when membranes are reduced during sealing and the measurement of the hydrogen production rate. During the measurements, we flowed 80% H_2/balance He on the oxygen-permeate side of the membrane and N_2 (pH_2O=0.49 atm) on the hydrogen-generation side. At 900°C, BFZ0 gave the highest hydrogen production rate (6.9 cm^3/min-cm^2) that we have measured with an OTM of comparable thickness.

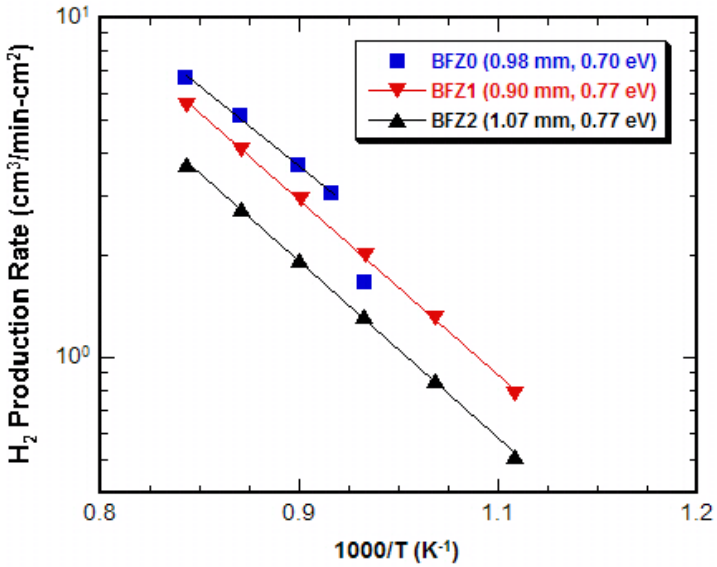

Fig. 12 Hydrogen production rate (normalized for 1.0 mm thickness) of BFZ0, BFZ1, and BFZ2 disks versus inverse temperature, measured with 80% H_2/balance He on oxygen-permeate side and N_2 (pH_2O=0.49 atm) on hydrogen-generation side. Inset gives actual thickness and apparent activation energy.

Like its oxygen permeation flux, BFZ0's hydrogen production rate shows a change in slope at ≈750-775°C. We discontinued the hydrogen production rate measurements below 750°C, because He leakage increased abruptly, possibly due to a volume change caused by a phase transition. To test the alternative possibility that the leakage resulted from a poor seal, the sample was heated again to the sealing temperature (≈950°C), but the leakage did not decrease. Unlike BFZ0, neither BFZ1 nor BFZ2 showed a distinct change in the slope of hydrogen production rate versus temperature. Similar to the trend in oxygen flux measurements, increasing the substitution of Zr for Fe decreased the hydrogen production rate due to a decrease in oxygen conductivity. The activation energies for oxygen permeation were 0.26, 0.31, and 0.36 eV for BFZ0, BFZ1, and BFZ2, respectively, and the activation energies for the hydrogen production rate were approximately double the values for oxygen permeation. As was observed with the oxygen flux measurements, the level of zirconium doping had little effect on the apparent activation energy for hydrogen production.

Ba-Sr-Fe-O: Figure 13 shows oxygen flux as a function of inverse temperature for ≈1-mm-thick disks of BFO, BSFO, and SFO. The figure inset gives the measured membrane thickness and apparent activation energy for each sample. The activation energy for BFO was determined by using only the data for the cubic phase, i.e., at temperatures above the phase transition at ≈870°C. Above the phase transition, un-doped BFO gave the highest oxygen permeation flux. Substituting Sr for Ba appeared to lower the temperature of the cubic to low-symmetry phase transition, but it increased the apparent activation energy from 0.30 eV for BFO to 0.49 eV for BSFO and 0.77 eV for SFO. The oxygen flux of BSFO is similar to that of SFO at high temperature but becomes higher at low temperatures due to its lower activation energy.

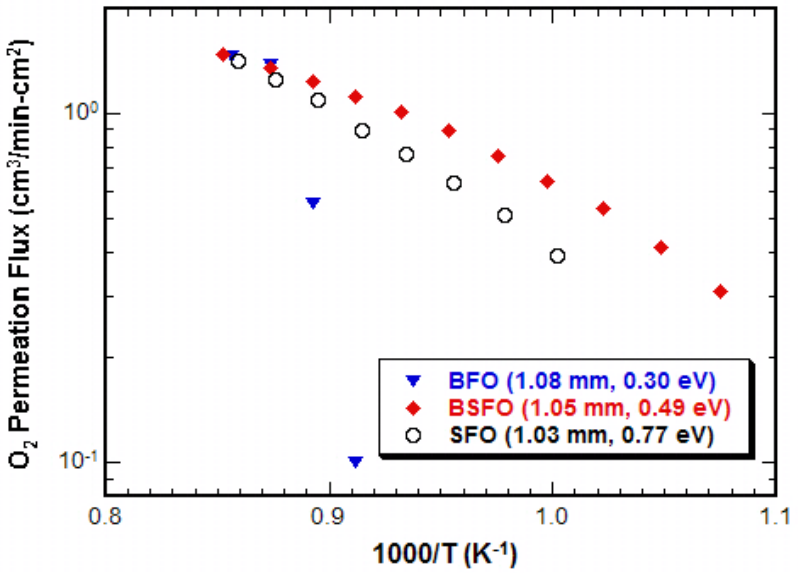

Fig. 13 Oxygen flux of BFO, BSFO, and SFO disks versus inverse temperature. Inset gives measured membrane thickness and apparent activation energy only above the phase transition (≈870°C) for BFO.

Findings from other studies suggest that BSFO's higher oxygen flux, compared to that of SFO, might be related to a higher oxygen vacancy concentration in BSFO. Shao et al. [13] observed an increase in the oxygen flux of $SrCo_{0.8}Fe_{0.2}O_3$ (SCFO) when Ba was substituted for Sr to make $Ba_{0.5}Sr_{0.5}Co_{0.8}Fe_{0.2}O_3$ (BSCFO). Thermogravimetric analysis (TGA) [14, 15] showed that the oxygen vacancy concentration of BSCFO is considerably higher than that of SCFO at 600-1000°C, even though a change in vacancy concentration is not expected because Sr and Ba have the same oxidation state. BSCFO's higher concentration of oxygen vacancies might be the reason its oxygen flux is higher than that of SCFO. Likewise, substituting Ba for Sr in SFO to produce BSFO might increase the oxygen flux by increasing the oxygen vacancies. And with its relatively low activation energy, BSFO might be useful for low-temperature OTM applications.

Ba-Sr-Cu-Fe-O: Based on the promising results reported by Efimov et al. [16], we tried to measure the oxygen flux of BSCF disks, but could not because they developed fine cracks after sintering. We were able, however, to measure the oxygen flux of BSCF/Ag composites with 10-40 vol.% Ag as a function of temperature. Composites with <30 vol.% Ag gave a slightly higher oxygen flux due to their higher volume fractions of the OTM, but we focused on composites with ≥30 vol.% Ag because the mechanical properties appeared to improve with the Ag content. Figure 14 shows the oxygen flux for an LSCF thin-film disk and thick (>0.5 mm) disks of LSCF, BFZ1, and BSCF/Ag composites. The figure inset gives the thickness of each OTM and the Ag content for the BSCF/Ag composites. At low temperatures (≤600°C), the oxygen flux for the BSCF/Ag disks was lower than that for the BFZ1 disk, but was higher than that for the LSCF disk and was similar to that for the much thinner LSCF thin-film disk. The comparable flux values for the LSCF thin-film disk and much thicker BSCF/Ag disks indicate that higher oxygen flux values should be achievable with BSCF/Ag thin films.

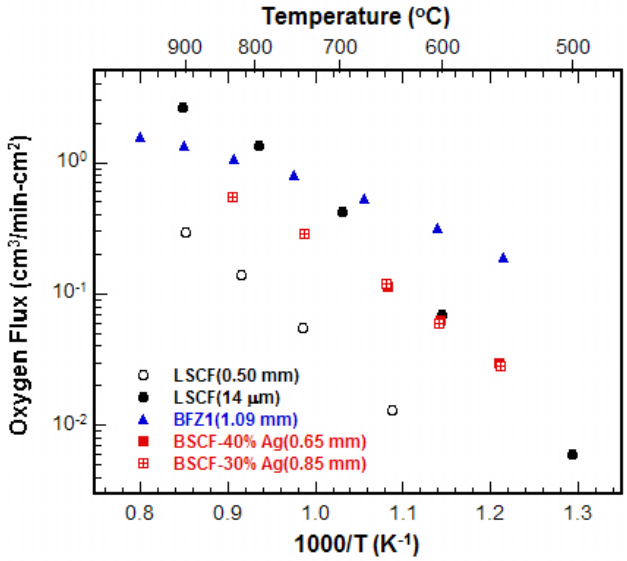

Fig. 14 Oxygen flux of various disk-type OTMs versus inverse temperature. The figure inset gives OTM composition, OTM thickness, and Ag content of BSCF/Ag composites.

In another approach to increase the hydrogen production rates at low temperatures (<700°C), we are developing techniques for fabricating OTM thin films on porous substrates. We prepared BFZ1 and BSCF/Ag (40 vol.%) thin films on substrates made from the same powders in order to achieve a good match in thermal expansion between the films and their substrates. To prepare porous BSCF/Ag substrates, we mixed the BSCF/Ag powder mixture with carbon powder (20 wt.%) in IPA, and the resulting mixture was ball-milled, dried, and screened. After screening, a disk (1-in. diameter) was uniaxially pressed and then sintered at 860°C for 10 h in ambient air. A slurry for preparing thin films was made by mixing the BSCF/Ag powder mixture with binder (polyvinyl butyral), plasticizer, and α-terpineol. One side of the disk was painted with the slurry and dried at 80°C for 1 h. After drying, the disk was sintered at 900°C for 7 h in ambient air. Similarly, BFZ1 thin films were prepared on BFZ1 substrates made from a powder mixture containing BFZ1 and carbon (15 wt.%). Then, the BFZ1 thin-film disks were sintered at 1290 °C for 6 h in ambient air.

To this point, we have not been able to produce satisfactory BFZ1 or BSCF/Ag thin films. Figure 15 shows a fracture surface and a plan view of BFZ1 thin films, and Fig. 16 shows similar views of a BSCF/Ag thin film. The BFZ1 thin film shown in Fig. 15a (thickness ≈15-20 μm) appeared reasonably dense with some isolated pores, and the substrate seemed to contain sufficient porosity for good gas transport. The plan view shows good grain development (grain size ≤40 μm), and the fracture surface shows a clear demarcation between the dense thin film and the porous substrate. The thickness of BFZ1 films was controllable and could be reduced to as little as ≈15 μm. Although their microstructure is acceptable, BFZ1 thin films have shown a tendency to crack during ethanol reforming conditions. The cause for this cracking is not known and will require further study.

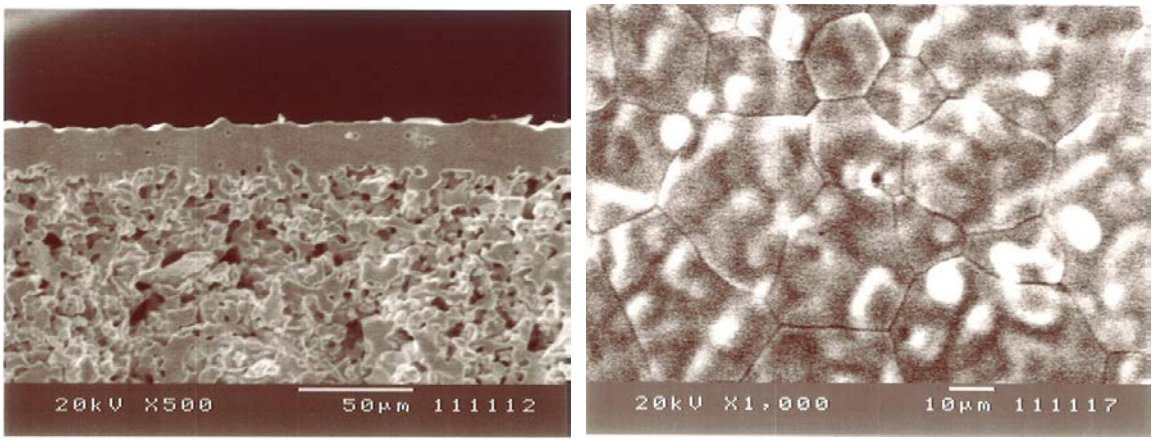

(a) (b)

Fig. 15 a) Fracture-surface and b) plan view of BFZ1 thin films on BFZ1 porous substrates.

The BSCF/Ag thin films prepared to date have been unacceptable due to excessive densification of the substrates. In contrast to BFZ1 films, BSCF/Ag films (Fig. 16) have shown no clear boundary between the substrate and film. A similar result was obtained when BSCF/Ag films were made on Ag-free BSCF substrates. Gas transport would be very limited through such a dense substrate, and the membrane's thickness would be essentially equivalent to that of the substrate and the film. To improve the properties of BSCF/Ag thin films, the substrates must be produced with more porosity without impeding densification of the thin film.

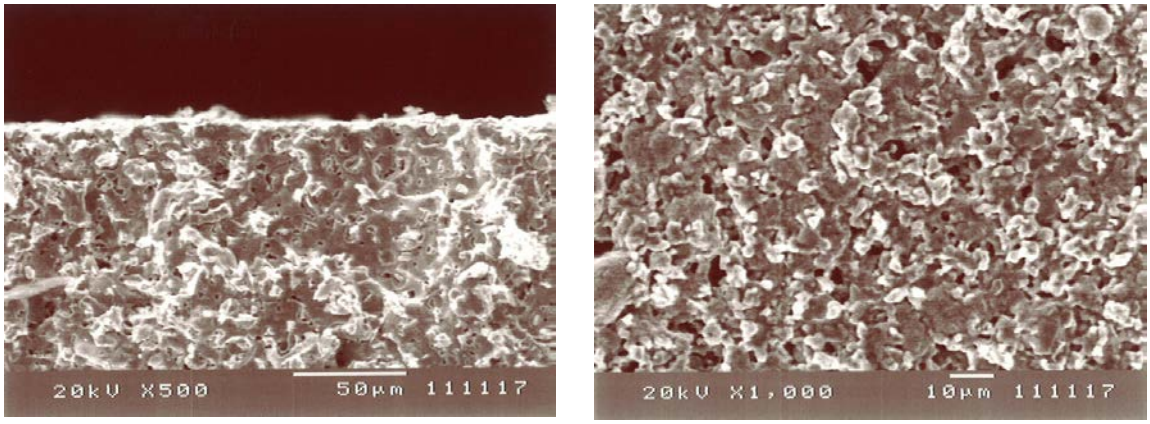

(a) (b)

Fig. 16 a) Fracture-surface and b) plan view of BSCF/Ag thin film on BSCF/Ag substrate.

V. FUTURE WORK

We will continue efforts to develop new OTM materials for producing hydrogen via coal/coal gas-assisted water splitting. In these efforts, we will investigate new membrane compositions and apply methods described in this report to enhance the hydrogen production rate of the OTMs being developed. Based on the principles of solid-state chemistry, we will prepare and test novel materials thought to have potential for high hydrogen production rates. To increase the hydrogen production rates of existing OTM materials, we will continue to improve methods for reproducibly fabricating membranes with thickness less than ≈25 μm, and we will coat membranes with porous layers, working to optimize the microstructural features of the porous layers, such as porosity and pore size. When the hydrogen production rate is significantly influenced by sintering conditions, we will optimize the sintering process to enhance hydrogen production.

We will fabricate and test tubular thin-film OTMs to demonstrate that OTMs with a significant hydrogen production rate are practical for large-scale industrial applications. Tubes are practical for large-scale industrial processes due to their large active area and the relative ease of their fabrication and gas-manifolding. To enhance the hydrogen production rates of tubular thin films, we will develop methods to coat both of the tube's surfaces with porous layers.

Thin-film OTM tubes will be used to demonstrate that the products from coal combustion can drive hydrogen production via water dissociation. In this concept, coal is combusted on one side of an OTM while hydrogen is produced on the other side via water splitting. This concept increases process efficiency by reducing the number of steps needed to produce hydrogen from coal. In this concept, the hydrogen produced is physically separated from carbon dioxide and all other impurities; therefore, hydrogen purification is simpler and more cost-effective. Gas separation costs would be reduced, because the OTM contains no precious metals. Because coal combustion is exothermic, it would supply heat that is required for water splitting. In addition, the CO_2-rich waste stream from the proposed process would be ideal for sequestration. We will use CO/CO_2 gas mixtures to test the feasibility of this concept at low temperatures ($\leq$700°C). The concept was demonstrated at low temperatures using LSCF thin-film disks with CO/CO_2 gas mixtures simulating a coal combustion atmosphere, but tests with LSCF thin-film tubes failed when the tubes cracked. To prevent cracks in LSCF thin-film tubes during tests at low temperatures, modifications will be made in the processing and/or testing of the tubes. If cracking of LSCF thin-film tubes appears to be unavoidable, alternative OTM compositions will be tested.

Good chemical stability is a critical requirement for OTMs due to the high temperatures and corrosive environments they will encounter; therefore, we will continue evaluating the chemical stability of OTMs. We will test the chemical and mechanical stability of OTMs in longer (up to ≈1000 h) exposures to industrially useful conditions, e.g., the atmospheres and temperatures that are typical for coal combustion and coal gasification. We will study the effect of syngas components on the hydrogen production rate of OTMs with and without H_2S in the gas. To assess the extent and course of reaction between the membrane and the atmosphere, the microstructure of membranes will be examined before and after exposures to industrial conditions.

Finally, we will evaluate process issues and economics as technical progress warrants. As directed by NETL's program managers, we will make contacts and hold discussions with potential collaborators. We will work with NETL's in-house R&D team and their Systems Engineering group to validate the process concept and assess the techno-economics of using OTMs to produce hydrogen by water splitting. We will provide technical input and engineering data to the NETL team to develop models for process viability and for thermal management studies.

PUBLICATIONS AND PRESENTATIONS

Hydrogen Production by High-Temperature Water Splitting Using Mixed Oxygen Ion-Electron Conducting Membranes, Proc. 201st Electrochem. Soc. Mtg., Philadelphia, PA, May 12-17, 2002.

Method for Generating Hydrogen by Catalytic Decomposition of Water, U.S. Patent 6,468,499, Oct. 22, 2002.

Hydrogen Production by Water Splitting Using Mixed Conducting Membranes, Proc. National Hydrogen Assoc. 14th Annual U.S. Hydrogen Meeting, Washington, DC, March 4-6, 2003.

Hydrogen Production by Water Dissociation Using Mixed-Conducting Membranes, presented at 225th Amer. Chem. Soc. Natl. Mtg., Fuel Chemistry Div., New Orleans, March 23-27, 2003.

Hydrogen Production by Water Dissociation Using Oxygen-Permeable Cermet Membranes, presented at 105th Ann. Mtg. of Amer. Ceram. Soc., Nashville, April 27-30, 2003.

Hydrogen Production by Water Dissociation Using Mixed Conducting Membranes, presented at Second Information Exchange Meeting on Nuclear Production of Hydrogen, Argonne Natl. Lab., Oct. 2-3, 2003.

Use of Mixed Conducting Membranes to Produce Hydrogen by Water Dissociation, Intl. J. of Hydrogen Energy, 29, 291-296 (2004).

Hydrogen Production from Water Splitting Using Mixed Oxygen Ion-Electron Conducting Membranes, U.S. Patent 6,726,893, Apr. 27, 2004.

Hydrogen Production by Water Dissociation Using Mixed-Conducting Ceramic Membranes, Proc. of National Hydrogen Association's 15th Annual U.S. Hydrogen Energy Conf., Los Angeles, CA, April 27-30, 2004.

Hydrogen Production from Water Using Mixed-Conducting Ceramic Membranes, presented at 15th World Hydrogen Energy Conf., Yokohama, Japan, June 27-July 2, 2004.

Development of Dense Ceramic Membranes for Hydrogen Production and Separation, presented at American Soc. for Materials--Annual Materials Solution Conf., Columbus, OH, Oct. 18-21, 2004.

Hydrogen Production by Water Splitting Using Dense Thin-Film Cermet Membranes, presented at Fall Meeting of Materials Research Society, Boston, Nov. 28-Dec. 2, 2005.

Hydrogen Production by Water Dissociation Using Mixed Oxygen Ion-Electron Conducting Membranes, presented at Electrochem. Soc. 2005 Fall Mtg., Los Angeles, Oct. 16-21, 2005.

Hydrogen Production by Water Dissociation Using Mixed-Conducting Dense Ceramic Membranes, invited presentation at Amer. Chem. Soc. 231st Natl. Mtg., Atlanta, March 26-30, 2006.

Hydrogen Production by High-Temperature Water Splitting Using Electron-Conducting Membranes, U.S. Patent 7,087,211, Aug. 8, 2006.

Mixed-Conducting Membranes for Hydrogen Production and Separation, presented at 2006 MRS Fall Meeting, Boston, MA, Nov. 27 - Dec 1, 2006.

Hydrogen Production by Water Dissociation Using Mixed-Conducting Dense Ceramic Membranes, Intl. J. of Hydrogen Energy, 32, 451 (2007).

Reforming of Natural Gas via Water Splitting Using Dense Ceramic Membranes, presented at Natl. Hydrogen Assoc. Meeting, San Antonio, TX, March 19-22, 2007.

Hydrogen Production by Water Splitting Using Mixed Ionic-Electronic Conducting Membranes, presented at 211th Meeting of Electrochem. Soc., Chicago, IL, May 6-10, 2007.

Hydrogen Production by Reforming of Natural Gas via Water Splitting using Dense Ceramic Membranes, presented at Intl. Symposium on Materials Issues in a Hydrogen Economy, Richmond, VA, Nov. 12-15, 2007.

Hydrogen Production by Water Dissociation Using Oxygen Transport Membranes, presented at 213th Electrochemical Soc. Meeting, May 18-23, 2008, Phoenix, Arizona.

$La_{0.7}Sr_{0.3}Cu_{0.2}Fe_{0.8}O_{3-x}$ as Oxygen Transport Membrane for Producing Hydrogen via Water Splitting, presented at 213th Electrochemical Soc. Meeting, Phoenix, Arizona, May 18-23, 2008.

Hydrogen Production from Fossil and Renewable Sources Using an Oxygen Transport Membrane, Intl. J. Hydrogen Energy, 35, 4103 (2010).

REFERENCES

[1] U. Balachandran, *Argonne National Laboratory Hydrogen Separation Membranes--Annual Report for FY 2003*.

[2] U. Balachandran, *Argonne National Laboratory Hydrogen Separation Membranes--Annual Report for FY 2002*.

[3] S. Ihara, Bull. Electrotech. Lab., 41, 259-280 (1977).

[4] B. Ma and U. Balachandran, Ceram. Trans., 73, 169-177 (1997).

[5] P. S. Maiya, U. Balachandran, J.T. Dusek, R.L. Mieville, M.S. Kleefisch and C.A. Udovich, Solid State Ionics, 99, 1-7 (1997).

[6] L. Qiu, T. H. Lee, L.-M. Liu, Y. L. Lang, and A. J. Jacobson, Solid State Ionics, 76, 321-329 (1995).

[7] T. H. Lee, Y. L. Lang, A. J. Jacobson, B. Abeles, and M. Zhou, Solid State Ionics, 100, 77-85 (1997).

[8] H. Naito and H. Arashi, Solid State Ionics, 79, 366-370 (1995).

[9] U. Balachandran, *Argonne National Laboratory Hydrogen Separation Membranes--Annual Report for FY 2008, ANL-09/08*.

[10] C.Y. Park, T. H. Lee, S. E. Dorris, and U. Balachandran, Int. J. Hydrogen Energy, 35, 4103-4110 (2010).

[11] K. Watanabe, D. Takakuch, M. Yuasa, T. Kida, K. Shimano, Y. Teraoka, and N Yamazoe, J. Electrochem. Soc., 156, E81, 2009.

[12] X. Zhu, Y. Cong, and W. Yang, J. Membr. Sci., 283, 158, 2006.

[13] J. P. Shao, W. S. Yang, Y. Cong, H. Dong, J. H. Tong, and G. X. Xiong, J. Membr. Sci., 172, 177 (2000).

[14] L. M. Liu, T. H. Lee, L. Qiu, Y. L. Yang, and A. J. Jacobson, Mater. Res. Bull. 31, 29 (1996).

[15] J. F. Vente, S. McIntosh, W. G. Haije, and H. J. M. Bouwmeester, J. Solid State Electrochem., 10, 581 (2006).

[16] K. Efimov, T. Halfer, A. Kuhn, P. Heitjans, J. Caro, and A. Feldhoff, Chem. Mater., 22, 1540-1544 (2010).

Energy Systems Division
Argonne National Laboratory
9700 South Cass Avenue, Bldg. 212
Argonne, IL 60439-4838

www.anl.gov